A Robust and Rapid Camera Calibration Method by One Captured Image

Jin Zhang, Huan Yu, Huaxia Deng, *Member, IEEE*, Zhiwen Chai, Mengchao Ma, and Xiang Zhong

***Abstract*— A robust and rapid camera calibration method is essential in vision measurement. This paper proposes a camera calibration method using a 2.5-D coding target that requires just a single captured image and is capable of identifying the intrinsic and extrinsic parameters of a camera system simultaneously. The calibration target consists of four fixed planes to which coded patterns are attached. The fixed planes of the target prevent the ill condition that arises in Zhang's method, and they provide four different homography matrices at the same time. The extrinsic parameters of the cameras are calculated using the geometric constraints of the feature circles on each plane. The coded pattern allows the four planes to be distinguished automatically. The proposed method is first verified by comparison experiments with three classical calibration methods. The results confirm that the proposed method has the greatest accuracy and smallest variance of errors. The influences on the calibration results of geometric parameters such as the dihedral angle and the area ratio of the feature circles are then investigated by systematic experiments. This proposed camera calibration method using a single captured image represents a breakthrough in a camera calibration technology and has a broad potential for application to machine vision and vision measurement.**

***Index Terms*— Camera calibration, ill-conditioned system, rapid, robust, target.**

I. Introduction

CAMERAS are the most important sensors in machine vision, which has a wide range of applications in artificial intelligence [1]–[3], vision measurement [4]–[8], and robotics technology [9]–[11]. Camera calibration is a crucial aspect of this technique and involves the rapid construction of accurate geometric relationships among different coordinates. Rapidity, robustness, and accuracy are three major challenges faced by camera calibration methods in vision measurement.

Many calibration methods have been proposed to deal with these three challenges. From a mathematical point of view, calibration methods can be categorized depending on whether they are based on a linear or nonlinear model. The linear calibration method uses the original pinhole camera model to establish the relationship among the image coordinate system, the camera coordinate system, and the world coordinate system. The relevant parameters are obtained in a simple and rapid manner by solving linear equations, but the resulting accuracy is poor because of neglecting lens distortion [12]–[15]. To increase the accuracy of calibration results, a nonlinear method taking account of lens imperfections was presented in the manual edited by Slama [16]. However, with this method, the parameters are extracted with difficulty and the processing speed is slow. The method is also sensitive to the selection of initial values and noise. With a nonlinear calibration method, it is not guaranteed that the parameters will converge to the global optimal solution. To combine the advantages of the linear model and the nonlinear model, Tsai [17] proposed a two-step method based on a radial alignment constraint. In this method, the intrinsic parameters are obtained by a linear calculation. The remaining parameters are calculated using a nonlinear optimization process excluding the translation of the camera in the direction of the optical axis. The increased accuracy of this method is achieved at the cost of lower speed and the imposition of stringent requirements on the equipment employed. This method is not suitable for use with cameras that exhibit complex distortions. The convergence of the results depends on the initial values. Heikkila and Silven [18] improved the two-step method by compensating for distortion caused by circular features and using a linear method to solve for the parameters of the inverse model. However, the explicit calibration method with a complex interpolation algorithm reduces computational speed, and the high sensitivity to initial values decreases the robustness of the results.

To enhance the robustness of calibration results and reduce the complexity of the equipment required, Zhang [19] proposed checkerboard calibration, which requires four corners and at least three poses of the target. The original solution for the camera parameters is calculated using a linear model, and then, the nonlinear maximum likelihood method is used for nonlinear refinement after taking the objective function of the lens distortion into consideration. This method gives accurate results for a prepared target, but the calibration process is time consuming when there are a large number of cameras, and the robustness of the parameters is affected by the target position. There have been a variety of modifications of Zhang's method. Bell *et al.* [20] developed an accurate method for calibrating an out-of-focus camera by using the carrier phase pattern in a display. However, the calibration process is no simpler, and the ill condition of the method when calibrated by a plane

Manuscript received June 3, 2018; revised November 8, 2018; accepted November 13, 2018. Date of publication December 17, 2018; date of current version September 13, 2019. This work was supported in part by the National Natural Science Foundation of China under Grant 51675156, Grant 51575156, Grant 51775164, and Grant 51705122, in part by the Aviation Science Fund under Grant 201719P4, and in part by the Fundamental Research Funds for the Central Universities under Grant JZ2017HGPA0165 and Grant PA2017GDQT0024. The Associate Editor coordinating the review process was Jochen Lang. *(Corresponding author: Huaxia Deng.)*

The authors are with the School of Instrument Science and Optoelectronics Engineering, Hefei University of Technology, Hefei 230009, China (e-mail: hxdeng@hfut.edu.cn).

Color versions of one or more of the figures in this article are available online at http://ieeexplore.ieee.org.

Digital Object Identifier 10.1109/TIM.2018.2884583

target remains. Also, extrinsic parameters are not considered in this method. Albarelli *et al.* [21], Huang *et al.* [22], and Jia *et al.* [23] presented improvements that dramatically reduce the reprojection error, but without any increases in the robustness or speed of the process. Liu *et al.* [24] substituted laser spots for the corners of a plane target to enhance the robustness of extracting feature points under complex light conditions in outdoor environments, and Schmalz *et al.* [25] used a high-resolution digital display as an active calibration target to obtain more accurate results. However, neither of these methods increase the speed of calibration, nor do they provide a complete solution to the problem of robustness. Identification of camera parameters requires several images of a plane target at different distances, which limits the speed of calibration when the number of cameras increases.

The speed of calibration is dependent on the degree of automation and the simplicity of the operating process during calibration experiments [26]. The number of captured images is directly related to the speed of calibration. Many researchers have proposed targets of different dimensions to enhance robustness and improve the rapidity of camera calibration. A 1-D target was first proposed by Zhang [27] in order to simplify the calibration of multiple cameras by means of a closed-form solution requiring more than six poses of the target. This approach solves the problem of view blocking by the surrounding camera array. However, unintended movement of the fixed point can lead to the failure of calibration. The robustness and the accuracy of calibration using a 1-D target are still poorer than those achievable with plane targets. A particular combination of 1-D objects designed by Miyagawa *et al.* [28] can be used to calibrate extrinsic camera parameters with a single target image, although the accuracy of the camera parameters obtained by this single-path calibration is sensitive to image noise. Zhao and Li [29] and Mitchelson and Hilton [30] proposed a method that acquires 600 frames of a moving wand to solve the fixed-point problem with a 1-D target. However, because of the inherent nature of 1-D targets, it is a very challenging task to improve the robustness and accuracy of the calibration results that they provide. A 3-D target design called an inward-looking visual sensor network was presented by Shen and Hornsey [31] to calculate all the parameters of a camera from a single image. However, their method does not employ any nonlinear optimization step to estimate lens distortion, and the orientation of the outer targets with respect to the camera leads to errors in the intrinsic parameters. In addition, the robustness of this method is influenced by the stability of the images of the absolute conic.

In order to simplify the operating process, some calibration methods based on geometrical relationships in the images have been proposed. Such methods are more flexible, but cannot calibrate the full set of camera parameters in a single process. Barreto and Araujo [32], Ying and Hu [33], and Zou and Li [34] proposed catadioptric calibration methods to calibrate the intrinsic parameters on the basis of geometrical constraints of spheres. The external parameters of the cameras have not been considered in these works. The estimated intrinsic parameters depend on the accuracy of the extracted cones, resulting in a sensitivity to environmental noise. A similar method for rapid real-time calibration using an unknown scene was proposed by Luong and Faugeras [35]. Melo *et al.* [36] estimated the distortion parameters and intrinsic parameters by a geometric method, calibrating a camera using a minimum of three imaged lines from one image. However, the accuracy of the results was unsatisfactory. Li and Li [37] presented a panoramic stereo imaging system to measure depth information for vision over a full 360°.

The precision of 3-D reconstruction is influenced by a variety of factors. Some camera parameters and the positional relationship between camera and mirror must be known in advance. Schoepflin and Dailey [38] used this method to estimate lane boundaries and the vanishing points of lines along a roadway. However, the camera parameters cannot be identified for scenes that do not include clear parallel lines of a road, and the results include only focal length, down angle, and pan angle. To solve the problem of extracting line constraints from actual scenes, feature points that are easier to track in videos can be used for calibration. Nister [39] and Crandall *et al.* [40] presented a real-time calibration method using structure-from-motion (SFM) systems that calibrate extrinsic parameters only. However, robustness of automated SFM systems depends on the robustness of the feature point detection method, which is very difficult to achieve for scenes that are composed of objects with weak textures.

In general, for vision measurements, a method that can calibrate both intrinsic and extrinsic parameters robustly and rapidly is still lacking. This paper presents a new calibration method that attempts do so using a single captured image and with an accuracy comparable to that of Zhang's method. The proposed method calibrates the intrinsic parameters of a camera system using a single captured image of a target, and it provides three homography matrices simultaneously. The extrinsic parameters of the camera system can be calibrated by four points in the same image. The specific design of the target endows this calibration method with good robustness.

The remainder of this paper is organized as follows. Section II describes the principles of the proposed method. Section III presents the design of the 2.5-D coding target and the calibration procedures for the method. Section IV describes comparison experiments to systematically investigate the robustness and accuracy of the method. Section V presents the results of these experiments. Section VI gives conclusions.

II. Principles

A. Calibration Procedures

The frameworks of the calibration procedures of the proposed method are shown in Fig. 1. The designed target is first placed in the cameras field of view without precise adjustment of the target or changes in pose. Then, a single image of the target is taken by the cameras under the control of a workstation. Finally, the spatial coordinates of the feature points and the pixel coordinates of the feature points extracted from the image are combined to calculate the camera parameters. The calibration results consist of the intrinsic parameters, the extrinsic parameters between the two cameras, and the distortion coefficients. The calibration process does not require the operator to move the target several times, in contrast to

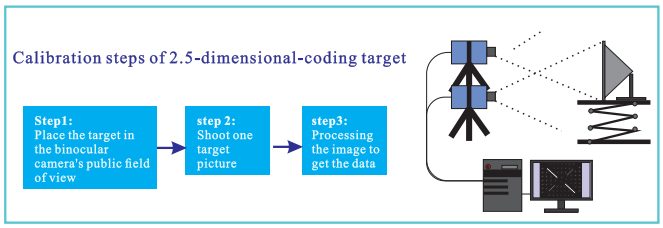

Fig. 1. Calibration procedures of the proposed method.

Zhang's method with checkerboard target. Because of the fixed structure of each surface of the 2.5-D coding target, inaccuracies in calibration results due to improper operation are avoided. In contrast to methods using a classic plane calibration target, the proposed method needs only a single captured image for calibration, making its operation rapid and simple and capable of a high degree of automation.

B. Single-Camera Model

To tackle the three challenges facing camera calibration technology, this paper investigates the principle of Zhang's method further. The essential reason for ill-conditioned equations, which leads to numerical instability in any algorithm, can be found in the mathematical model of the cameras. The ill-conditioned equations are analyzed under different situations. The particular structure of the 2.5-D coding target is designed such that ill-conditioned equations do not have any effect on calibration results and also to simplify the process of camera calibration. The principle of the proposed calibration method is as follows. With $\mathbf{H}_i$ denoting the homography matrix resolved from the ith pose of a plane target and $\mathbf{I}$ denoting the intrinsic camera parameter matrix, the relationship between $\mathbf{H}_i$ and $\mathbf{I}$ is

$$\mathbf{H}_i = \gamma\,\mathbf{I}[\mathbf{r_{i1}}\quad \mathbf{r_{i2}}\quad \mathbf{t_i}] = [\mathbf{g_{i1}}\quad \mathbf{g_{i2}}\quad \mathbf{g_{i3}}] = \begin{bmatrix} h_{i1} & h_{i2} & h_{i3} \\ h_{i4} & h_{i5} & h_{i6} \\ h_{i7} & h_{i8} & h_{i9} \end{bmatrix} \tag{1}$$

where γ is a scale factor, $\mathbf{r}_{i1}$ and $\mathbf{r}_{i2}$ are the rotation vectors, and $\mathbf{t}_i$ is a translation vector. The following two constraint relationships can be obtained from the orthogonality between $\mathbf{r}_{i1}$ and $\mathbf{r}_{i2}$:

$$\begin{cases} \mathbf{g}_{i1}^{\mathrm{T}}\mathbf{I}^{-\mathrm{T}}\mathbf{I}^{-1}\mathbf{g}_{i2} = \mathbf{0} \\ \mathbf{g}_{i1}^{\mathrm{T}}\mathbf{I}^{-\mathrm{T}}\mathbf{I}^{-1}\mathbf{g}_{i1} = \mathbf{g}_{i2}^{\mathrm{T}}\mathbf{I}^{-\mathrm{T}}\mathbf{I}^{-1}\mathbf{g}_{i2}. \end{cases} \tag{2}$$

The matrix $\mathbf{B} = \mathbf{I}^{-\mathrm{T}}\mathbf{I}^{-1}$ is symmetric and the six unique parameters of $\mathbf{B}$ can be written as a vector $\mathbf{b_i}$, $i \in \{1, 2, 3, 4, 5, 6\}$

$$\mathbf{b} = \begin{bmatrix} \mathbf{b}_1 & \mathbf{b}_2 & \mathbf{b}_3 & \mathbf{b}_4 & \mathbf{b}_5 & \mathbf{b}_6 \end{bmatrix}. \tag{3}$$

According to (1)–(3), it satisfies

$$\begin{cases} \mathbf{v}_{i1}^{\mathrm{T}}\mathbf{b} = \mathbf{0} \\ (\mathbf{v}_{i2} - \mathbf{v}_{i3})^{\mathrm{T}}\mathbf{b} = \mathbf{0} \end{cases} \tag{4}$$

where $\mathbf{v}_{ij}$, $j \in \{1, 2, 3\}$, are calculated from $\mathbf{H}_i$ as

$$\begin{cases} [\mathbf{v}_{i1}] = [h_{i1}^2 \quad 2h_{i1}h_{i2} \quad h_{i2}^2 \quad 2h_{i1}h_{i3} \quad 2h_{i2}h_{i3} \quad h_{i3}^2], \\ [\mathbf{v}_{i2}] = [h_{i1}h_{i4} \quad h_{i1}h_{i5} + h_{i2}h_{i4} \quad h_{i2}h_{i5} \quad h_{i3}h_{i4} + h_{i1}h_{i6} \\ \qquad\qquad h_{i3}h_{i5} + h_{i2}h_{i6} \quad h_{i3}h_{i6}] \\ [\mathbf{v}_{i3}] = [h_{i4}^2 \quad 2h_{i4}h_{i5} \quad h_{i5}^2 \quad 2h_{i4}h_{i6} \quad 2h_{i5}h_{i6} \quad h_{i6}^2]. \end{cases} \tag{5}$$

After calculation of the matrix $\mathbf{B}$, the matrix $\mathbf{I}$ is solved by singular value decomposition. The extrinsic parameters can then be calculated. They are $\mathbf{r}_1 = \gamma\,\mathbf{I}^{-1}\mathbf{b}_1$, $\mathbf{r}_2 = \gamma\,\mathbf{I}^{-1}\mathbf{b}_2$, $\mathbf{r}_3 = \mathbf{r}_1 \times \mathbf{r}_2$, and $\mathbf{t} = \gamma\,\mathbf{I}^{-1}\mathbf{b}_3$. The extrinsic parameters between the target coordinate system and the camera coordinate system are consisted of the rotation matrix $\mathbf{R} = \begin{bmatrix} \mathbf{r}_1 & \mathbf{r}_2 & \mathbf{r}_3 \end{bmatrix}$ and the translation vector $\mathbf{t}$.

The camera distortion model is then established as

$$\begin{aligned} x_c &= x + x(k_1 r^2 + k_2 r^4) + 2p_1 y + p_2(r^2 + 2x^2) \\ y_c &= y + y(k_1 r^2 + k_2 r^4) + 2p_2 x + p_1(r^2 + 2y^2) \end{aligned} \tag{6}$$

where (x, y) are the original coordinates of a point on the image plane, and (x_c, y_c) are the coordinates of the point after distortion correction. k_1 and k_2 are the radial distortion coefficients, and p_1 and p_2 are the tangential distortion coefficients.

After the camera parameters have been determined, they are optimized by maximum likelihood estimation. There are four planes in the 2.5-D coding target, and each plane has n points. The measured image point coordinates are affected by independent and identically distributed noise. The quantity to be optimized is

$$\sum_{i=1}^{4}\sum_{1}^{n} \|\mathbf{P}_{ij} - \hat{\mathbf{P}}(\mathbf{A}, \mathbf{R}_i, \mathbf{t}_i, \mathbf{Q}_j, k_1, k_2, p_1, p_1)\|^2 \tag{7}$$

where $\hat{\mathbf{P}}(\mathbf{A}, \mathbf{R}_i, \mathbf{t}_i, \mathbf{Q}_j)$ is the projection of the point $\mathbf{Q}$ in the images. Lens distortion is taken into account while optimizing.

C. Stereo Model

According to the above-mentioned formulations, the parameters of the single camera are calculated. With $\mathbf{R}_l$ (respectively, $\mathbf{R}_r$) and $\mathbf{T}_l$ (respectively, $\mathbf{T}_r$) denoting the rotation matrix and the translation vector between the coordinate system of the left camera $\mathbf{C}_l$ (respectively, the right camera $\mathbf{C}_r$) and the coordinate system of the fixed target, the relationship between the coordinate systems of the left and right cameras can be expressed as follows:

$$\begin{aligned} \delta\mathbf{C}_l &= \begin{bmatrix} \mathbf{R}_l & \mathbf{t}_l \\ 0 & 1 \end{bmatrix}\begin{bmatrix} \mathbf{R}_r & \mathbf{t}_r \\ 0 & 1 \end{bmatrix} \\ \mathbf{C}_r &= \begin{bmatrix} \mathbf{R}_l\mathbf{R}_r & \mathbf{R}_l\mathbf{t}_r + \mathbf{t}_1 \\ 0 & 1 \end{bmatrix}\mathbf{C}_r \end{aligned} \tag{8}$$

where δ is a scale factor.

D. Analysis and Solution of the Ill-Conditioned System of the Camera Model

There are two constraint relationships between $\mathbf{b}$ and $\mathbf{H}_i$. The matrix $\mathbf{b}$ contains five unknown values. At least three different $\mathbf{H}_i$ are required to solve for $\mathbf{b}$. To simplify the calculation process, the unknown quantities in the matrix $\mathbf{b}$ are solved by establishing linear equations, and three groups of known volume are provided by three $\mathbf{H}_i$. Analysis of the robustness properties of Zhang's method then reveals the

reason for the ill-conditioned nature of the equations

$$\begin{bmatrix} \mathbf{v}_{11}^{\mathrm{T}} \\ (\mathbf{v}_{12}-\mathbf{v}_{13})^{\mathrm{T}} \\ \mathbf{v}_{21}^{\mathrm{T}} \\ (\mathbf{v}_{22}-\mathbf{v}_{23})^{\mathrm{T}} \\ \mathbf{v}_{31}^{\mathrm{T}} \\ (\mathbf{v}_{32}-\mathbf{v}_{33})^{\mathrm{T}} \end{bmatrix} \mathbf{b} = \mathbf{C}\mathbf{b} = \mathbf{0}. \tag{9}$$

The number of conditions imposed on the coefficient matrix $\mathbf{C} = \left[\mathbf{c}_1\ \mathbf{c}_2\ \mathbf{c}_3\ \mathbf{c}_4\ \mathbf{c}_5\ \mathbf{c}_6\right]^{\mathrm{T}}$ provides a criterion for determining whether the equations are ill-conditioned. The equation is regarded as ill conditioned when this number $\mathrm{cond}(\mathbf{C})$ is large. Otherwise, the equation is well-conditioned. The number $\mathrm{cond}(\mathbf{C})$ is given by

$$\mathrm{cond}(\mathbf{C}) = \|\mathbf{C}\|\|\mathbf{C}^{-1}\| = \frac{\|\mathbf{C}\|\|\mathbf{C}^{*}\|}{|\det \mathbf{C}|} \tag{10}$$

where $\|\mathbf{C}\|$ is the infinity norm of $\mathbf{C}$. In the matrix $\mathbf{C}$, there must exist a group of real numbers k^n that satisfy the formula $\sum_1^n k^n \mathbf{c}_n = \mathbf{b}$, where $\mathbf{b}$ is the optimal approximation of the vector $\mathbf{c}_n$. The degree of correlation among the vectors $\mathbf{c}_n$ is defined as $\mathbf{r}(\mathbf{c}_1, \mathbf{c}_2, \ldots, \mathbf{c}_n) = \mathbf{r}(\mathbf{c}_n, \mathbf{b})$; then, the following hold.

1) If $\mathbf{b} = \mathbf{c}_n$, then $\mathbf{r}(\mathbf{c}_1, \mathbf{c}_2, \ldots, \mathbf{c}_n) = 1$. The vectors $\mathbf{c}_n$ are linearly correlated with each other. In this case, $|\det \mathbf{C}| = 0$.
2) If $\mathbf{b} \to \mathbf{c}_n$, then $\mathbf{r}(\mathbf{c}_1, \mathbf{c}_2, \ldots, \mathbf{c}_n) \to 1$. The vectors $\mathbf{c}_n$ are strongly correlated with each other. In this case, $|\det \mathbf{C}| \to 0$.
3) If $\mathbf{b} \perp \mathbf{c}_n$, then $\mathbf{r}(\mathbf{c}_1, \mathbf{c}_2, \ldots, \mathbf{c}_n) = 0$. The vectors $\mathbf{c}_n$ are orthogonal to each other. In this case, $|\det \mathbf{C}|$ is a large number.

In the first case, the worst situation is that $\mathbf{b}$ cannot be solved by the equation when $|\det \mathbf{C}| = 0$. It follows from the relation between $\mathbf{c}_n$ and $\mathbf{H}_i$ that $\mathbf{r}(\mathbf{c}_1, \mathbf{c}_2, \ldots, \mathbf{c}_n)$ is equal to 1. In other words, $\mathbf{H}_i$ are linearly correlated with each other. The second case indicates that (10) tend to infinity when $|\det \mathbf{C}|$ goes to zero and the equation becomes an ill-conditioned system, which leads to poor robustness results. The strong relationship among $\mathbf{H}_i$ is caused by the tiny changes in the pose of the target that occur during the calibration process. In this case, $\mathbf{r}(\mathbf{c}_1, \mathbf{c}_2, \ldots, \mathbf{c}_n)$ goes to zero.

Finding the source of the abnormal solution and eliminating the factors responsible is a common approach to improving the stability of engineering systems. Therefore, this paper deals with the factor that leads to the ill-conditioned equation by designing a 2.5-D coding target. This target provides four different $\mathbf{B}_{ij}$ without linear correlation at a given time.

$\mathbf{Q}_1 \in \triangle\mathrm{OAB}$, $\mathbf{Q}_2 \in \triangle\mathrm{OBC}$, $\mathbf{Q}_3 \in \triangle\mathrm{OCD}$, and $\mathbf{Q}_4 \in \triangle\mathrm{ODA}$ are the coordinate vectors of feature points in different planes of the 2.5-D coding target, and $\mathbf{P}_1$, $\mathbf{P}_2$, $\mathbf{P}_3$, and $\mathbf{P}_4$ are the corresponding pixel coordinate vectors. The structure of the proposed 2.5-D coding target is shown in Fig. 2. It is in the shape of a right square pyramid, and the feature points are in the four side planes. Four plane-coordinate systems are established in each part of the target. The dihedral angle θ expresses the linear correlation among the four plane-coordinate systems and is a condition for judging whether the calibration system is ill-conditioned. Because the four planes of the proposed target are not coplanar, it is guaranteed that the matrix $\mathbf{I}$ can be solved from the equations. By contrast, Zhang's method provides only one $\mathbf{H}$ from a single image of the plane target, and because of the randomly changing pose of the target the existence of a nonlinear relationship between each $\mathbf{H}$ cannot be ensured.

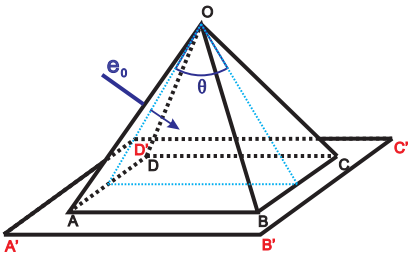

(a)

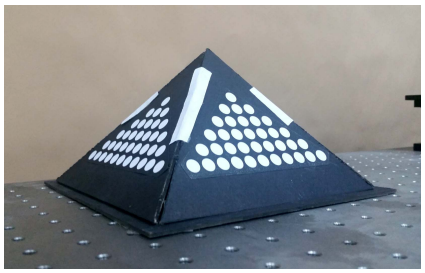

(b)

Fig. 2. Structure of the 2.5-D coding target. (a) Schematic diagram. (b) Photograph [41].

E. Extraction of Feature Points

The stereo structure of the 2.5-D coding target leads to a slight defocus on the target surface out of the focal plane. In the case of slight defocus and a low-light environment, the feature circle used in this paper is more easily detected than an angle point. Therefore, a circular pattern is chosen here as the characteristic pattern of the 2.5-D coding target. The center of the circle in the image of the target is extracted by the centroid algorithm. The pixel point of the circle is (u_i, v_i) $(i \in \mathbf{Z}, 1 \le i \le \mathbf{N})$ and the pixel set of the circle is $\mathbf{C}_p$, $(u_i, v_i) \in \mathbf{C}_p$. The pixel coordinate of the circle center is (u_c, v_c), where

$$u_c = \frac{1}{n}\sum_{i=1}^{n} u_i, \quad v_c = \frac{1}{n}\sum_{i=1}^{n} v_i. \tag{11}$$

III. Calibration Method

A. Structure of the 2.5-D Coding Target

The structure of the proposed 2.5-D coding target is designed in the form of a rectangular pyramid OABCD for investigating the relationship between the dihedral angle of the 2.5-D coding target, as shown in Fig. 2(a). The normal vector e_0 of the plane including $\triangle$ABC points to the side with a cyclic array, and θ expresses the dihedral angle of the two sides in the normal direction. Fig. 2(b) is a picture of the proposed target. The joints between two planes have different sizes of rectangles, which are the coding elements

Fig. 3. Coded pattern on the target plane.

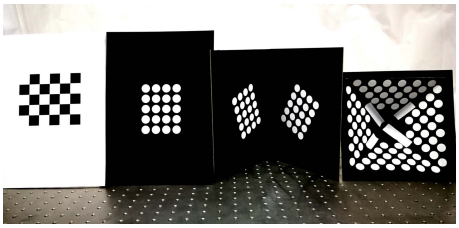

Fig. 4. Four kinds of target (from left to right): checkerboard target, single-plane–circle target, biplane–circle target, and 2.5-D coding target.

used for distinguishing the four planes. The feature pattern is shown in Fig. 3. The rectangles are larger than the feature circles. The four rectangles can be distinguished by their area. The linear equation determined by the central coordinates of the two bigger rectangles can be expressed as $y = a_1x + b_1$ and that determined by the central coordinates of the two smaller rectangles as $y = a_2x + b_2$. The center coordinate of the feature circle is written as (x_i, y_i). Circles belonging to different planes are separated into four parts by the two lines.
If $y_i < a_1x_i + b_1$ and $y_i < a_2x_i + b_2$: $(x_i, y_i) \in \mathbf{A_1}$.
If $y_i < a_1x_i + b_1$ and $y_i > a_2x_i + b_2$: $(x_i, y_i) \in \mathbf{A_2}$.
If $y_i > a_1x_i + b_1$ and $y_i < a_2x_i + b_2$: $(x_i, y_i) \in \mathbf{A_3}$.
If $y_i > a_1x_i + b_1$ and $y_i > a_2x_i + b_2$: $(x_i, y_i) \in \mathbf{A_4}$.
$\mathbf{A_1}$, $\mathbf{A_2}$, $\mathbf{A_3}$ and $\mathbf{A_4}$ mean the sets of characteristic circle in the same plane of the 3-D coding target. The 2.5-D coding target is a single-sided black hard cardboard sheet of thickness 3 mm. The surface of the cardboard is quite flat. The positional relationships among the feature points in different planes are indeterminate, but those of points in the same plane are known.

IV. Experiments

A. Experiment Using a Target With Different Planes

To verify the robustness and accuracy of the proposed method, four kinds of target are used to calibrate the same camera system. Fig. 4 shows the four kinds of target, which all have the same numbers of feature circles in each plane. The diameter of each circle is 16 mm and the center-to-center distance is 20 mm. There are 20 circles in each plane. The checkerboard target has 20 corners, and the side length of each square is 20 mm. The extrinsic parameters relating the camera and the target change along with the pose of the target. A binocular camera system consisting of two fixed cameras is used to compare the stability and accuracy of the extrinsic parameters.

The experimental setup is shown in Fig. 5. Two industrial CMOS cameras produced by IO industries are installed in two stands that are fixed on the optical platform. The pixel size is 5.5 μm and the image pixel size is 1024×1280. The focal length of the lens is 12 mm. The targets are placed on an adjustable-height lift used as a support. An annular light source compensates for light, and an image acquisition workstation is used to control the cameras. After the cameras have been installed, the 2.5-D coding target is moved until it comes into the middle of the field of view of the two cameras. Each camera then takes simultaneous images of the target.

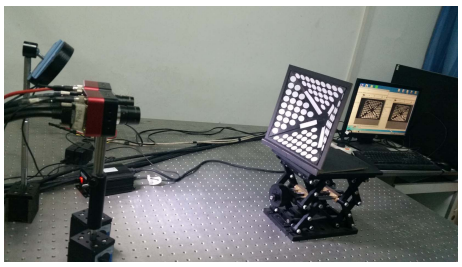

Fig. 5. Experimental setup.

Each target is calibrated 10×. The 2.5-D coding target can be calibrated by a single image. The single-plane–circle and checkerboard targets need at least four different images, and the biplane–circle target needs at least two. To ensure that each calibration data point has the same number of feature points, the comparison experiments choose one image for the proposed method, two for the biplane–circle target, four for the single-plane–circle target, and four for the checkerboard target to calibrate the cameras. The ground truth of the calibration is the result of Zhang's method using 20 images calculated using the MATLAB calibration toolbox. The accuracy of the calibration results is indicated by the relative errors of the calibrated parameters. The relative errors in focal length f, rotation matrix $\mathbf{R}$, translation vector $\mathbf{T}$, and the principal points (c_x, c_y) are shown in Figs. 10 and 11. It should be noted that the principal point error is calculated as

$$e_c = \frac{\sqrt{(c'_x - c_x)^2 + (c'_y - c_y)^2}}{\sqrt{c_x^2 + c_y^2}} \tag{12}$$

where (c'_x, c'_y) are the calibration results and (c_x, c_y) is the ground truth. The rotation matrix error is [42]

$$e_r = \frac{\|\mathbf{R}'_q - \mathbf{R}_q\|}{\|\mathbf{R}_q\|} \tag{13}$$

where $\mathbf{R}'_q$ is the normalized quaternion of the calibrated rotation matrix $\mathbf{R}'$, while $\mathbf{R}_q$ is the normalized quaternion of the ground truth of the rotation matrix $\mathbf{R}$. The global optimization includes the distortion model. The camera parameters after distortion correction are contrasted and analyzed in the contrast experiment.

B. Experiment Using Targets With Different Dihedral Angles

The proposed 2.5-D coding target provides information on four planes at the same time, which allows the camera parameter calibration to be performed using a single image. The dihedral angle of the target will influence the calibration results. For example, if the dihedral angle were 180°, the proposed target would reduce to a single plane target. Thus, the

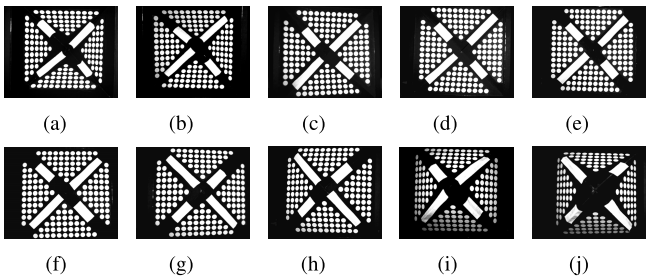

Fig. 6. Targets with different dihedral angles. (a) 80°. (b) 100°. (c) 120°. (d) 140°. (e) 160°. (f) 200°. (g) 220°. (h) 240°. (i) 260°. (j) 280°.

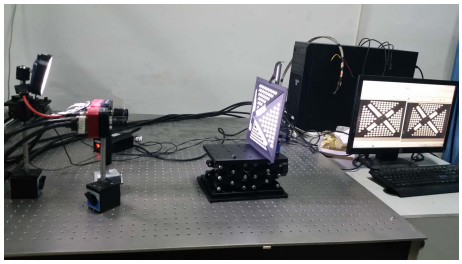

Fig. 7. Target with 220° dihedral angle.

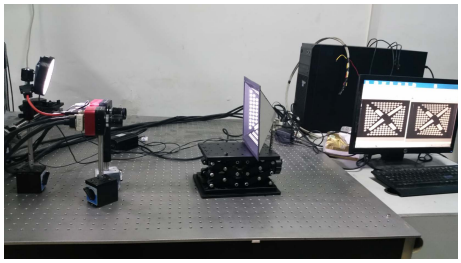

Fig. 8. Target with 100° dihedral angle.

relationship between the dihedral angle of the 2.5-D coding target and the calibration results is studied by comparison experiments. Ten different dihedral angles are chosen to calibrate the camera system under the same conditions: 80°, 100°, 120°, 140°, 160°, 200°, 220°, 240°, and 280°. Fig. 6 shows the images of the target with different dihedral angles. Each target has the same triangular pattern array consisting of 36 circles in each plane. The diameter of each circle is 10 mm and the distance between two adjacent centers is 12 mm.

It should be noted that the target changes from concave to convex when the dihedral angle becomes greater than 180°, as demonstrated in Figs. 7 and 8. The aim of this experiment is to explore the impact of the dihedral angle on the accuracy and robustness of the calibration results. As in the previous experiments, the influence on the relative errors and variances of the focal length f, rotation matrix $\mathbf{R}$, translation vector $\mathbf{T}$, and the principal points (c_x, c_y) are investigated.

C. Experiment Using Targets With Different Feature Point Sizes

For a plane target with circular feature points, the size of these points has been found to affect the accuracy of the calibration results [43]. To study the effects of the size of the feature circles on calibration results for the proposed method, comparison experiments are carried out. To ensure

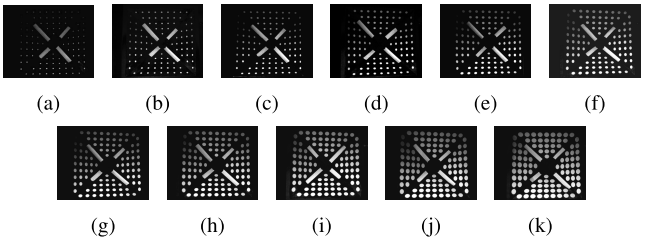

Fig. 9. Targets with different sizes of feature circles. (a) 4 mm. (b) 5 mm. (c) 6 mm. (d) 7 mm. (e) 8 mm. (f) 9 mm. (g) 10 mm. (h) 11 mm. (i) 12 mm. (j) 13 mm. (k) 14 mm.

TABLE I
DISTORTION COEFFICIENTS OF THE RIGHT CAMERA

	k_1	k_2	p_1	p_2
Ground truth	−0.19003	0.40412	0.00187	0.00545
Single	−0.15211	0.32471	0.00120	0.00295
Biplane	**−0.16375**	0.43691	0.00144	0.00394
2.5D	−0.16257	**0.41326**	**0.00208**	0.00371
Checkerboard	−0.14832	0.39018	0.00291	**0.00520**

TABLE II
DISTORTION COEFFICIENTS OF THE LEFT CAMERA

	k_1	k_2	p_1	p_2
Ground truth	−0.20357	0.32741	−0.00132	0.00516
Single	−0.18910	0.27385	−0.00171	0.00557
Biplane	−0.17841	**0.3523**	−0.00177	**0.00508**
2.5D	**−0.19084**	0.27935	**−0.00140**	0.00469
checkerboard	−0.17742	0.23501	−0.00162	0.00458

that the diameter of the feature circle is the only variable in the experiment, the feature pattern consists of a triangular array of 25 circles with the same circular distance of 18 mm and the dihedral angle of the target remains at 120°. The distance between the target and the camera system is constant. The diameters of the feature circles range from 4 to 14 mm in the intervals of 1 mm. The corresponding ratios of the area of the feature circles to the field of view are 1.0‰, 1.4‰, 1.9‰, 2.5‰, 3.1‰, 3.8‰, 5.1‰, 6.0‰, 7.0‰, 8.1‰, and 9.2‰. Images of the targets with different sizes of feature circles are shown in Fig. 9.

V. RESULTS AND DISCUSSION

A. Accuracy and Robustness Analysis

To identify the accuracy and robustness of the proposed method, four different camera calibration methods are compared in the contrast experiment. The distortion coefficients of the right and left cameras calibrated by different methods are shown in Tables I and II, respectively. The ones closest to the ground truth are highlighted as bold in Tables I and II. The right camera's distortion coefficient results, which are presented in Table I, show that the result of k_1 and p_1 calibrated by the proposed method and k_2 and p_2 calibrated by the double-sided target are closest to the true value. The result of checkerboard calibrated k_1 and p_2 are the worst, and p_1 calibrated by the two sided targets is also the worst. The distortion coefficient table of the left camera shows that k_1, k_2, and p_1 calibrated by the proposed method and p_2 calibrated by the checkerboard target are closest to the true value. k_1 and p_1 calibrated by the checkerboard target and k_2 and p_2 calibrated

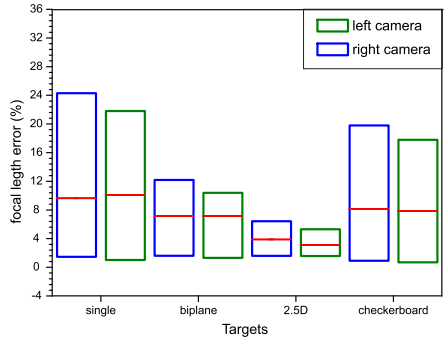

(a)

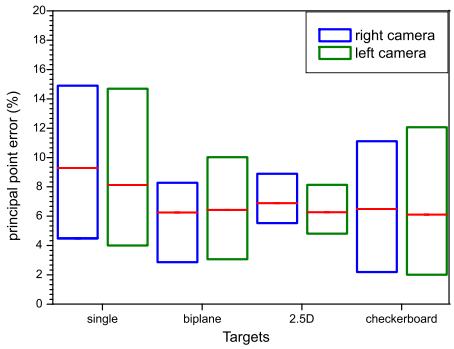

(b)

Fig. 10. Intrinsic parameters calibrated by four methods. (a) Focal length error. (b) Principal point error.

by the single target are the worst. Generally, the proposed method calibrates the distortion coefficients accurately. Fig. 10 shows the intrinsic parameters. The boundaries of the blue boxes indicate the error ranges, which represent the robustness, and the red lines indicate the average value of the errors, which reflects the accuracy. Among the four calibration methods examined, the proposed method has the smallest error range, while the largest average error is that for the single-plane–circle target. As shown in Fig. 10(a), the average error in the focal length calibrated by the proposed method is about 3%, which is the smallest average error among the four methods. The average error for the checkerboard target is close to 8%, and the error range of the calibration using this target is more than three times greater than that with the proposed method. The single-plane–circle target has the greatest average error and the greatest error range, both of which are close to the result obtained using the checkerboard target. The biplane target has an average error of about 7% and the error range is smaller than the two methods with plane target. Fig. 10(b) shows the principal point error of the cameras. The proposed 2.5-D coding target, the biplane target, and the checkerboard target have almost the same average principal point error, about 7%, while the error range with the proposed target is the smallest, which shows that this is the most robust method. The single-plane–circle has the greatest average error. Both of the methods with plane targets have poor robustness.

The errors in the extrinsic parameters are shown in Fig. 11. The proposed method is the most robust and accurate. The average translation errors for the single-plane–circle target are

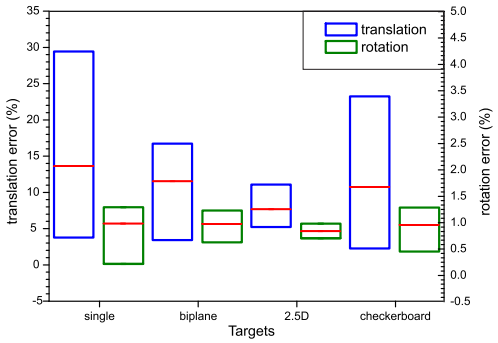

Fig. 11. Extrinsic parameters calibrated by four methods.

the worst in terms of robustness and accuracy. The average translation errors for the checkerboard and biplane target have almost the same values. The average translation errors calculated for the 2.5-D coding target are less than 10%, with a range from 6% to 11%. The average errors for the other three methods are greater than 10%. However, the biplane target has an average error smaller than the two methods with plane targets. The rotation errors for all the methods are low. The average rotation error is less than 1% for all the methods. In particular, the average rotation error of the 2.5-D coding target is about 0.8%, with a range from 0.72% to 0.95%, which is also the most robust and accurate result.

Overall, the proposed method using a 2.5-D coding target is the most rapid calibration method compared with the other three methods, requiring only a single shot. It has the smallest range of parameter variation, which indicates that it is the most robust. This method is also very accurate in calibrating both the intrinsic and extrinsic parameters. For the intrinsic parameters, the accuracy of the proposed method is similar to that of the popular checkerboard target. For the extrinsic parameters, the proposed method has the smallest average error. Thus, it is a rapid, robust, and accurate method. Furthermore, the calibration process is automated, with no manual operation being required throughout the calibration process. It should be noted that the robustness of calibration method increases with the number of the fixed plane, because the target with fixed planes avoids the ill condition in the calibration process.

B. Impact of Structural Parameters

The proposed target has two major structural parameters: the dihedral angle and the size of the feature circles. The four fixed planes of the proposed target allow the method to calibrate using a single image. Therefore, it is important to reveal the influence of the dihedral angle on the calibration results. To find the relationship between the dihedral angle and the calibration results, eleven 2.5-D coding targets with different dihedral angles are used to calibrate the cameras. Fig. 12 shows the relationship between the dihedral angle and the errors in the intrinsic parameters. The errors in the intrinsic parameters decrease when the dihedral angle moves away from 180°. From Fig. 12(a), it can be seen that the focal length error of the right camera is greater than 4% for dihedral angles from 140° to 240°, while the error of the left camera increases considerably from 0.3% to 3.8% at 160°. From Fig. 12(a),

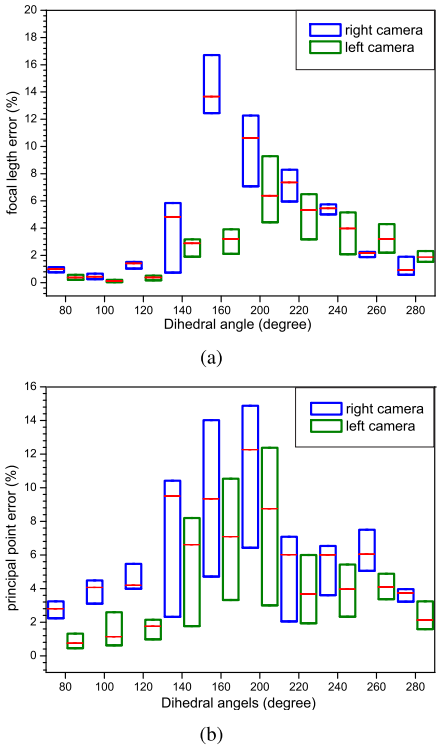

Fig. 12. Results for intrintsic parameters with different dihedral angles. (a) Focal length error. (b) Principal point error.

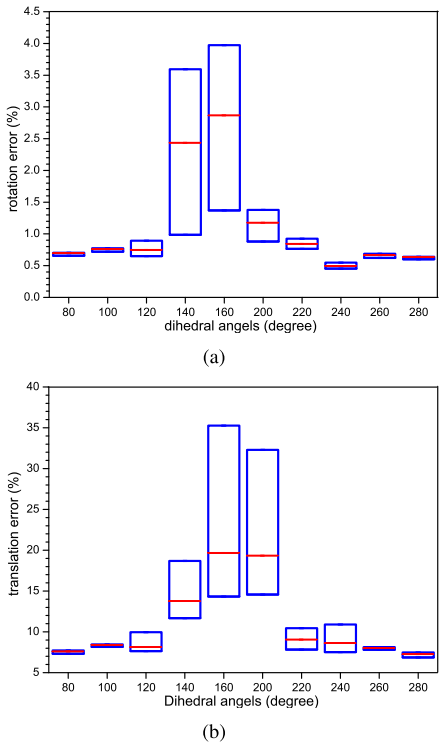

Fig. 13. Results for extrinsic parameters with different dihedral angles. (a) Rotation error. (b) Translation error.

it can be seen that the error in the principal point is greater than 6% for dihedral angles from 140° to 200°. Both the accuracy and robustness of the principal point are improved outside the range from 140° to 200°. The extrinsic parameters exhibit the same tendency, as shown in Fig. 13. Outside the range from 140° to 220°, the average error remains small and the robustness increases. In Fig. 13(a), the average error of rotation remains below 1% from 80° to 120° and from 220° to 280°. In Fig. 13(b), the average translation error is greater than 10% from 140° to 200°.

These results show that the 2.5-D coding target with dihedral angle outside the range from 140° to 220° gives calibration results with improved accuracy and robustness. This conclusion will be important for the further design and practical application of this type of target.

The feature size is the other structural parameter. To study the effect of feature size on the calibration results, eleven 2.5-D coding targets with different sizes of feature circle are selected to calibrate the camera system. As shown in Fig. 14(a), the focal length error decreases abruptly at a diameter of 10 mm (5.1‰ ratio of feature circle area to field of view). The error decreases with increasing diameter when the diameter is larger than 9 mm (3.8‰). However, the error remains high at about 9% before the rapid decrease. In Fig. 14(b), it can be seen that the principal point error has no obvious relationship with the diameter of the feature points. However, the error of the left camera is smallest for a diameter of 10 mm (5.1‰). In Fig. 15(a), the rotation parameter is insensitive to the size of the circular features. However, the error range becomes smaller when the diameter increases. This means that the robustness of the

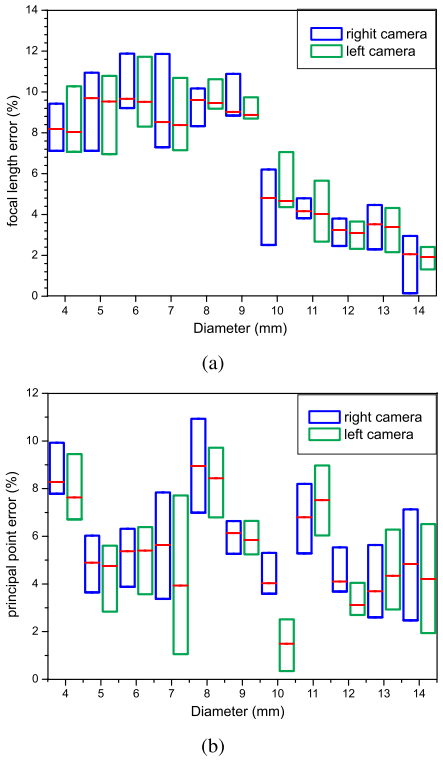

Fig. 14. Results for intrintsic parameters with different sizes of feature circle. (a) Focal length error. (b) Principal point error.

rotation is affected by the diameter of the feature circle. The proposed targets with larger feature circles are more robust than those with smaller circles. Fig. 15(b) shows the influence of feature size on the translation error. The error is around 10.5% for feature sizes from 4 mm (1.0‰) to 9 mm (3.8‰),

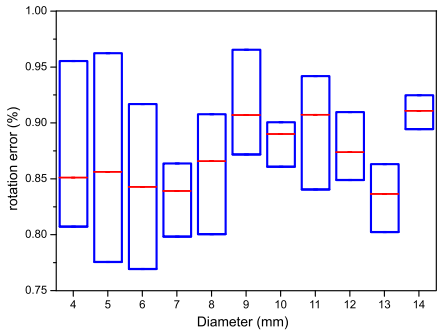

(a)

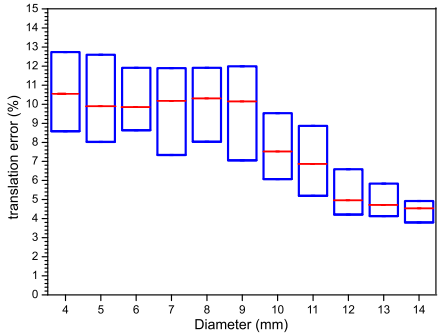

(b)

Fig. 15. Extrinsic parameters results with different sizes of feature circle. (a) Rotation error. (b) Translation error.

and the error range also remains at the same level. However, both the average error and the variation in the error decrease with increasing feature size in the range from 10 mm (5.1‰) to 14 mm (9.2‰), and this change tends to be stable after a size of 11 mm (6.0‰).

These results show that some of the calibration parameters are influenced by the size of the feature circle. This affects the accuracies of the focal length and the translation. The robustness of the rotation is improved with increasing feature size. The principal point is closest to the ground truth for a 10 mm (5.1‰) feature circle. This discovery is important for guiding the calibration process of camera systems. Priority should therefore be given to increasing the size of the feature circle in the production of calibration targets to help reduce errors in calibration results.

VI. Conclusion

A rapid, robust, and accurate method for camera calibration has been proposed. This method is capable of calibrating all of the camera parameters, including the distortion model, using a single shot. The four fixed planes of the proposed target avoid ill condition of the calibration by setting the dihedral angle to an appropriate value. In addition, a low computational criterion for determining whether the solution of the calibration model is ill-conditioned has been proposed. A single captured image has been found to be sufficient for calibration of the intrinsic and extrinsic parameters. The calibration error is less than 5% for the proposed method, which gives the most robust results from the comparison experiments. The accuracy of the extrinsic parameters is better than that from Zhang's method. Also the distortion coefficients k_1 and p_1 calibrated by the proposed method are most closed to the ground truth. The accuracy and robustness of the calibration parameters are improved when the dihedral angle is in the range from 80° to 140° or from 220° to 280°. The size of the feature circle has a strong influence on the translation and the focal length, but no obvious influence on other parameters. The use of a feature circle with a ratio of area to a field of view greater than 7.0‰ (diameter 12 mm) can improve the calibration results. Overall, the proposed method provides rapid and automated calibration with high accuracy and robustness and can be considered a significance in camera calibration technology. The proposed technology has a wide range of potential applications in artificial intelligence, machine vision, and robotics technology.

References

[1] H. Zhe and H. Yujiao, "Research on table tennis tactics based on artificial intelligence," *Agro Food Ind. Hi Tech*, vol. 28, no. 1, pp. 624–627, 2017.
[2] A. Graves, M. Liwicki, S. Fernández, R. Bertolami, H. Bunke, and J. Schmidhuber, "A novel connectionist system for unconstrained handwriting recognition," *IEEE Trans. Pattern Anal. Mach. Intell.*, vol. 31, no. 5, pp. 855–868, May 2009.
[3] S. Yeung, N. L. Downing, L. Feifei, and A. Milstein, "Bedside computer vision—Moving artificial intelligence from driver assistance to patient safety," *New England J. Med.*, vol. 378, no. 14, pp. 1271–1273, 2018.
[4] X. Huang, F. Zhang, H. Li, and X. Liu, "An online technology for measuring icing shape on conductor based on vision and force sensors," *IEEE Trans. Instrum. Meas.*, vol. 66, no. 12, pp. 3180–3189, Dec. 2017.
[5] K. Liu, H. Wang, H. Chen, E. Qu, Y. Tian, and H. Sun, "Steel surface defect detection using a new Haar–Weibull-variance model in unsupervised manner," *IEEE Trans. Instrum. Meas.*, vol. 66, no. 10, pp. 2585–2596, Oct. 2017.
[6] J. Zhang, P. Zhang, H. Deng, and J. Wang, "High-accuracy three-dimensional reconstruction of vibration based on stereo vision," *Opt. Eng.*, vol. 55, no. 9, p. 091410, 2016.
[7] T. M. Kanakam *et al.*, "Adaptable ring for vision-based measurements and shape analysis," *IEEE Trans. Instrum. Meas.*, vol. 66, no. 4, pp. 746–756, Apr. 2017.
[8] Y. Xu and J. M. W. Brownjohn, "Review of machine-vision based methodologies for displacement measurement in civil structures," *J. Civil Struct. Health Monitor.*, vol. 8, no. 1, pp. 91–110, 2018.
[9] P. Kahn, L. Kitchen, and E. M. Riseman, "A fast line finder for vision-guided robot navigation," *IEEE Trans. Pattern Anal. Mach. Intell.*, vol. 12, no. 11, pp. 1098–1102, Nov. 1990.
[10] Y. Kuno, Y. Okamoto, and S. Okada, "Robot vision using a feature search strategy generated from a 3D object model," *IEEE Trans. Pattern Anal. Mach. Intell.*, vol. 13, no. 10, pp. 1085–1097, Oct. 1991.
[11] J. Yang, D. Zhang, J.-Y. Yang, and B. Niu, "Globally maximizing, locally minimizing: Unsupervised discriminant projection with applications to face and palm biometrics," *IEEE Trans. Pattern Anal. Mach. Intell.*, vol. 29, no. 4, pp. 650–664, Apr. 2007.
[12] D. C. Brown, "Close-range camera calibration," *Photogramm. Eng.*, vol. 37, no. 8, pp. 855–866, 1971.
[13] Y. I. Abdelaziz, "Direct linear transformation from comparator coordinates in close-range photogrammetry," in *Proc. ASP Symp. Close-Range Photogram. Illinois*, 1971, pp. 1–18.
[14] O. Faugeras and G. Toscani, "The calibration problem for stereo," in *Proc. IEEE Conf. Comput. Vis. Pattern Recognit.*, vol. 42, no. 12, 1986, pp. 195–213.
[15] J. G. Fryer, "Lens distortion for close-range photogrammetry," *Photogramm. Eng. Remote Sens.*, vol. 52, no. 1, pp. 51–58, 1986.
[16] C. C. Slama, Ed., "Manual of photogrammetry," *Photogramm. Rec.*, vol. 20, no. 112, pp. 390–392, 2010.
[17] R. Y. Tsai, "A versatile camera calibration technique for high-accuracy 3D machine vision metrology using off-the-shelf TV cameras and lenses," *IEEE J. Robot. Autom.*, vol. 3, no. 4, pp. 323–344, Aug. 1987.
[18] J. Heikkila and O. Silven, "A four-step camera calibration procedure with implicit image correction," in *Proc. IEEE Comput. Soc. Conf. Comput. Vis. Pattern Recognit.*, Jun. 2002, p. 1106.

[19] Z. Zhang, "A flexible new technique for camera calibration," *IEEE Trans. Pattern Anal. Mach. Intell.*, vol. 22, no. 11, pp. 1330–1334, Nov. 2000.

[20] T. Bell, J. Xu, and S. Zhang, "Method for out-of-focus camera calibration," *Appl. Opt.*, vol. 55, no. 9, pp. 2346–2352, 2016.

[21] A. Albarelli, R. Emanuele, and A. Torsello, "Robust camera calibration using inaccurate targets," in *Proc. Brit. Mach. Vis. Conf. (BMVC)*, Aberystwyth, U.K., Aug./Sep. 2010, pp. 1–10.

[22] L. Huang, Q. Zhang, and A. Asundi, "Flexible camera calibration using not-measured imperfect target," *Appl. Opt.*, vol. 52, no. 25, pp. 6278–6286, 2013.

[23] Z. Jia *et al.*, "Improved camera calibration method based on perpendicularity compensation for binocular stereo vision measurement system," *Opt. Express*, vol. 23, no. 12, pp. 15205–15223, 2015.

[24] Z. Liu, Y. Yin, S. Liu, and X. Chen, "Extrinsic parameter calibration of stereo vision sensors using spot laser projector," *Appl. Opt.*, vol. 55, no. 25, pp. 7098–7105, 2016.

[25] C. Schmalz, F. Forster, and E. Angelopoulou, "Camera calibration: Active versus passive targets," *Opt. Eng.*, vol. 50, no. 11, p. 113601, 2011.

[26] Y. Q. Shi, C. K. Sun, B. G. Wang, P. Wang, and H. X. Duan, "A global calibration method of multi-vision sensors in the measurement of engine cylinder joint surface holes," *Key Eng. Mater.*, vols. 467–469, pp. 1182–1188, Feb. 2011.

[27] Z. Zhang, "Camera calibration with one-dimensional objects," *IEEE Trans. Pattern Anal. Mach. Intell.*, vol. 26, no. 7, pp. 892–899, Jul. 2004.

[28] I. Miyagawa, H. Arai, and H. Koike, *Simple Camera Calibration From a Single Image Using Five Points on Two Orthogonal 1-D Objects*. Piscataway, NJ, USA: IEEE Press, 2010.

[29] Y. Zhao and W. Li, "Self-calibration of a binocular vision system based on a one-dimensional target," *J. Mod. Opt.*, vol. 61, no. 18, pp. 1529–1537, 2014.

[30] J. Mitchelson and A. Hilton, "Wand-based multiple camera studio calibration," Centre Vis., Speech Signal Process., Guildford, U.K., Tech. Rep., 2008, pp. 1–30.

[31] E. Shen and R. Hornsey, "Multi-camera network calibration with a non-planar target," *IEEE Sensors J.*, vol. 11, no. 10, pp. 2356–2364, Oct. 2011.

[32] J. P. Barreto and H. Araujo, "Geometric properties of central catadioptric line images," in *Proc. Eur. Conf. Comput. Vis.*, 2002, pp. 237–251.

[33] X. Ying and Z. Hu, "Catadioptric camera calibration using geometric invariants," *IEEE Trans. Pattern Anal. Mach. Intell.*, vol. 26, no. 10, pp. 1260–1271, Oct. 2004.

[34] W. Zou and S. Li, "Calibration of nonoverlapping in-vehicle cameras with laser pointers," *IEEE Trans. Intell. Transp. Syst.*, vol. 16, no. 3, pp. 1348–1359, Jun. 2015.

[35] Q.-T. Luong and O. D. Faugeras, "The fundamental matrix: Theory, algorithms, and stability analysis," *Int. J. Comput. Vis.*, vol. 17, no. 1, pp. 43–75, 1996.

[36] R. Melo, M. Antunes, J. P. Barreto, G. Falcao, and N. Goncalves, "Unsupervised intrinsic calibration from a single frame using a 'plumb-line' approach," in *Proc. IEEE Int. Conf. Comput. Vis.*, Dec. 2013, pp. 537–544.

[37] W. Li and Y. F. Li, "Single-camera panoramic stereo imaging system with a fisheye lens and a convex mirror," *Opt. Express*, vol. 19, no. 7, pp. 5855–5867, 2011.

[38] T. N. Schoepflin and D. J. Dailey, "Dynamic camera calibration of roadside traffic management cameras for vehicle speed estimation," *IEEE Trans. Intell. Transp. Syst.*, vol. 4, no. 2, pp. 90–98, Jun. 2003.

[39] D. Nister, "An efficient solution to the five-point relative pose problem," *IEEE Trans. Pattern Anal. Mach. Intell.*, vol. 26, no. 6, pp. 756–770, Jun. 2004.

[40] D. J. Crandall, A. Owens, N. Snavely, and D. P. Huttenlocher, "SfM with MRFs: Discrete-continuous optimization for large-scale structure from motion," *IEEE Trans. Pattern Anal. Mach. Intell.*, vol. 35, no. 12, pp. 2841–2853, Dec. 2013.

[41] J. Zhang, "Analysis of calibration accuracy of cameras with different target sizes for large field of view," *Young Sci. Forum 2017*, vol. 10710, p. 10710, 2018.

[42] V. Lepetit, F. Moreno-Noguer, and P. Fua, "EP*n*P: An accurate O(n) solution to the P*n*P problem," *Int. J. Comput. Vis.*, vol. 81, no. 2, pp. 155–166, 2009.

[43] J. Heikkila, "Accurate camera calibration and feature based 3-D reconstruction from monocular image sequences," *Acta Univ. Oul.*, vol. 81, no. 2, pp. 155–166, 1997.

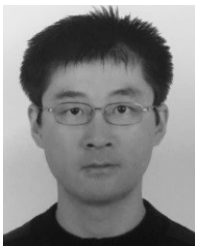

Jin Zhang received the B.E. degree from the Hefei University of Technology, Hefei, China, in 2005, and the M.S. and Ph.D. degrees from Tianjin University, Tianjin, China, in 2007 and 2010, respectively.

Since 2012, he has been an Associate Professor with the School of Instrument Science and Optoelectronics Engineering, Hefei University of Technology. His current research interests include optical measurement technology and vibration testing.

Dr. Zhang is a member of the Youth Committee of China Instrument and Control Society. He was a recipient of the second prize of the Science and Technology Award of the China Instrument and Control Society.

Huan Yu received the B.S. degree from the School of Instrument Science and Optoelectronics Engineering, Hefei University of Technology, Hefei, China, in 2015.

She is currently a Postgraduate Student with the School of Instrument Science and Optoelectronics Engineering, Hefei University of Technology. Her current research interests include vision measurement, camera calibration, and image processing.

Huaxia Deng received the B.E. and M.S. degrees from the University of Science and Technology of China, Hefei, China, in 2004 and 2007, respectively, and the Ph.D. degree from the University of Liverpool, Liverpool, U.K., in 2011.

Since 2012, he has been the Hungshan Young Scholar Professor with the School of Instrument Science and Optoelectronics Engineering, Hefei University of Technology. His current research interests include smart materials and vibration control.

Dr. Deng was elected as a member of the Institute of Physics in 2011. He was a recipient of the Duncan Norman Research Scholarship and the JinGuofan Prize for Excellent Youth of China Instrument Society. He is the Review Editor of the journal *Frontiers in Smart Materials*.

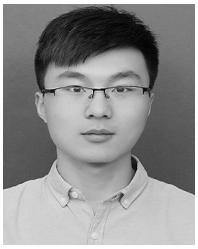

Zhiwen Chai received the B.S. degree from the School of Mechanical Engineering, Anhui University of Science and Technology, Huainan, China, in 2016.

He is currently a Postgraduate Student with the School of Instrument Science and Optoelectronics Engineering, Hefei University of Technology, Hefei, China. His current research interests include vision measurement and camera calibration.

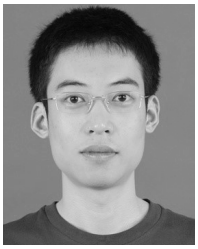

Mengchao Ma received the Ph.D. degree from the University of Science and Technology of China, Hefei, China, in 2014.

He is currently a Lecturer with the School of Instrument Science and Optoelectronics Engineering, Hefei University of Technology, Hefei. His current research interests include artificial compound eye, structured-light measurement, and dynamic testing.

Xiang Zhong received the B.S. degree from the School of Measurement and Control Technology and Instrument, Tianjin University, Tianjin, China, in 2008, and the Ph.D. degree in optical engineering from Beihang University, Beijing, China, in 2016.

He is currently a Lecturer with the School of Instrument Science and Optoelectronics Engineering, Hefei University of Technology, Hefei, China. His current research interests include optical fiber sensing and dynamic testing.